Eur. Phys. J. E (2019) **42**: 87
DOI 10.1140/epje/i2019-11851-6

THE EUROPEAN PHYSICAL JOURNAL E

Regular Article

Preliminary analysis of Diffusion Coefficient Measurements in ternary mIXtures 4 (DCMIX4) experiment on board the International Space Station*

A. Mialdun[1,a], H. Bataller[2], M.M. Bou-Ali[3], M. Braibanti[4], F. Croccolo[2], A. Errarte[3], J.M. Ezquerro[5], J.J. Fernández[5], Yu. Gaponenko[1], L. García-Fernández[2,6], J. Rodríguez[5], and V. Shevtsova[1]

[1] MRC, CP 165/62, Université libre de Bruxelles (ULB), 50, Ave. F.D. Roosevelt, B-1050 Brussels, Belgium
[2] Laboratoire des Fluides Complexes et leurs Réservoirs - IPRA UMR5150 E2S-Université de Pau et des Pays de l'Adour (UPPA) / CNRS / TOTAL, 1, Allée du Parc Montaury, 64600 Anglet, France
[3] Mechanical and Manufacturing Department, Mondragon Goi Eskola Politeknikoa (MGEP), Loramendi 4, Apdo. 23, 20500 Mondragon, Spain
[4] European Space Agency (ESA), ESTEC, Noordwijk, The Netherlands
[5] E-USOC, Ciencias y Operaciones Aeroespaciales, Universidad Politécnica de Madrid, Madrid, Spain
[6] Centre National d'Études Spatiales (CNES), 2, Place Maurice Quentin, 75001 Paris, France

Received 20 March 2019 and Received in final form 5 June 2019
Published online: 11 July 2019

Abstract. In the frame of the Diffusion Coefficient Measurements in ternary mIXtures 4 (DCMIX4) project the thermodiffusion experiments were conducted on the International Space Station (ISS) in the Selectable Optical Diagnostics Instrument (SODI) which is on orbit since 2009. We describe the results of the preliminary analysis of images downloaded during the execution of DCMIX4 in order to check the quality of the running experiments and, if needed, adjust the experiment parameters for the following runs. The quick analysis of raw data showed that they are meaningful and will allow to obtain the transport coefficients of examined ternary and binary mixtures.

1 Introduction

The thermodiffusion (Soret) effect and accompanying diffusion processes have been deeply investigated in the latest decades due to their inherent relation to fluid non-equilibrium thermodynamics and the underlying mechanisms, that are still poorly understood. Extended and well-established studies of the phenomena in binary mixtures have been performed [1–3], and now the interest focuses on the next, more complex step of assessing ternary mixtures [4–7].

The increasing interest of the international community in the subject has been further pushed due to the different microgravity activities developed by the European Space Agency (ESA). The need for microgravity experiments stems from the need of performing experiments in the absence of convective motions [8].

The aim of the "Diffusion Coefficient Measurements in ternary mIXtures" (DCMIX) series of experiments is to provide quantitative measurements of mass diffusion and Soret coefficients during thermodiffusion experiments on ternary mixtures performed in gravity-free environment. These series of experiments are performed on board the International Space Station (ISS) making use of the Selectable Optical Diagnostics Instrument (SODI), a facility installed within the Microgravity Science Glovebox (MSG) inside the Destiny U.S. Laboratory of the ISS. The analysis is performed by means of two-wavelength Mach-Zehnder optical interferometry in order to separate the concentration profiles for the two independent components of the mixtures. Up to now DCMIX1, DCMIX2 and DCMIX3 campaigns have already been completed and results have been published mostly for the first series of experiments [9–13]. All the cited three experimental campaigns involved ternary mixtures of three molecular liquids at various concentrations. This choice has the consequence that the mass diffusion coefficient matrix has two eigenvalues of similar value thus making particularly difficult to separate their contribution to the evolution of the

* Contribution to the Topical Issue "Thermal Non-Equilibrium Phenomena in Soft Matter", edited by Fernando Bresme, Velisa Vesovic, Fabrizio Croccolo, Henri Bataller.

[a] e-mail: amialdun@ulb.ac.be

system and even more difficult to extract the values of the non-diagonal elements of the diffusion matrix, as shown by the recent benchmark values for one of the DCMIX1 mixtures [14] and a recent analysis of optical measurements on ternary mixtures [12,15].

The ternary mixture toluene-methanol-cyclohexane is of fundamental interest as it exhibits a miscibility gap and a large region with negative Soret coefficients. The transport and optical properties of binary subsystems were extensively examined [16]. It is known from statistical physics for binary mixtures and confirmed experimentally for methanol + cyclohexane mixture [17], that the diffusion coefficient D drastically diminishes approaching the binodal and should be zero at spinodal, while the thermodiffusion coefficient D_T remains constant. As a consequence, the Soret coefficient $S_T = D_T/D$ should grow as $\sim 1/D$. A similar behaviour is expected in ternary systems, where one of the eigenvalues and the determinant of diffusion matrix should diminish and two Soret coefficients depend on the entire diffusion coefficients matrix. As a first approximation, one can guess that they grow as $S_{Ti} \sim 1/det$ where det is the determinant of the mass diffusion matrix. Previous measurements of the diffusion matrix for DCMIX2 samples indicated the decrease of the determinant as well as one of the eigenvalues approaching the demixing zone [18–20].

In addition, DCMIX2 data have revealed that approaching the demixing zone one of the Soret coefficients significantly increases. Unfortunately, the concentration of the mixtures was not stable in time due to poor compatibility of the sealing materials with liquids. Consequently, the evaluation of the exact values of the concentrations was ambiguous. Taking into account novelty and importance of the obtained results for the ternary mixture, three cells of DCMIX4 (1–3) have been filled with toluene-methanol-cyclohexane mixtures at concentrations different from those of DCMIX2 and closer to phase separation, in order to confirm the slowing-down of the mass diffusion and the divergence of the Soret coefficients. In fig. 1 the ternary composition map is reported including both the experimental points of the DCMIX2 campaign (shown by blue triangles) and the ones included in this new one (shown by red circles). As visible, the concentrations chosen for the DCMIX4 campaign are slightly closer to the demixing zone (shown as the shaded area) at small toluene concentration and all three mixtures have the same content of methanol (25% by mass). The analysis of the cells 1–3 has been coordinated by the team headed by V. Shevtsova (VS), from Université libre de Bruxelles (ULB), Belgium.

Another sample of DCMIX4 includes a mixture of fullerene-tetrahydronaphthalene-toluene, as the first complex mixture including nanoparticles. The results obtained by measuring this sample are expected to provide added value and a high impact in this very active research area with so many applications; advanced manufacturing, health, nanotechnologies and biotechnology [21–23]. The study of this sample has been coordinated by the team headed by M.M. Bou-Ali (MMBA), from Mondragon Goi Eskola Politeknikoa (MGEP), Spain.

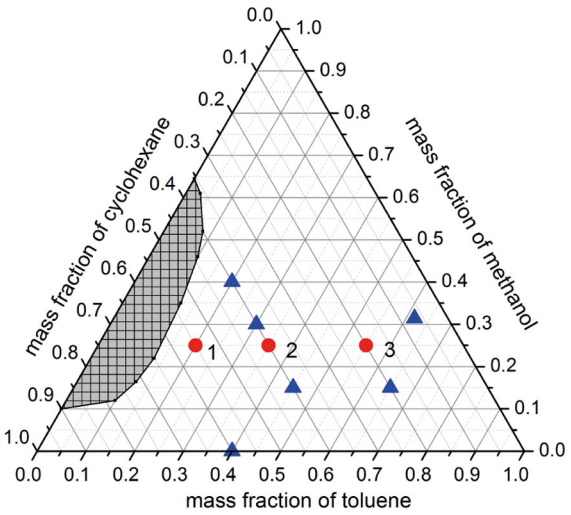

Fig. 1. Toluene-methanol-cyclohexane concentration map including samples from DCMIX2 (blue triangles) and DCMIX4 cells 1–3 (red circles). The hatched area indicates demixing zone at $T = 25\,^{\circ}\mathrm{C}$; the demixing zone expands as long as the temperature decreases.

The ternary mixture of polystyrene - toluene - cyclohexane has been chosen mainly because the two eigenvalues of the mass diffusion coefficients matrix are expected to be well separated, by a factor of about 10, as this mixture includes a polymer as one of the components, namely the polystyrene, having a much larger molecular weight than the other two [24]. This implies that the time evolution of the concentration profiles measured by SODI two-wavelength diagnostics will be easier to analyse and interpret, as the different contributions can be also separated on the basis of their kinetics. The binary mixture of polystyrene-toluene has been filled into the companion cell in order to establish reference values for the polymer in a molecular solvent. The binary sample is selected to be similar to the one used in the GRADFLEX space experiment [25,26], so that comparison will be performed between the results obtained through a totally different experimental approach. The analysis of cells 5–6 has been carried out by the team headed by H. Bataller (HB) and F. Croccolo (FC) from Université de Pau et des Pays de l'Adour (UPPA), France.

The sample content of all the cells is detailed in table 1. For component numbering, a hydrodynamic approach has been adopted, corresponding to a decreasing order of density; *i.e.* component 1 is the denser one and so on.

2 Experiment description

DCMIX4 cell array was delivered to the ISS inside the unmanned Cygnus cargo ship launched by the Antares rocket on 17th November 2018. It was installed inside SODI on Wednesday 12th December 2018 by the NASA astronaut Serena Auñón-Chancellor. The first scientific experiment started on 13th December 2018 and the tests continued

Table 1. List of liquid mixtures selected for the DCMIX4 cell array. The name of the coordinator is written after the cell number. Compositions of ternary mixtures are given in *percent* mass fractions.

Cell #	Component 1	Component 2	Component 3
1 (VS)	toluene	methanol	cyclohexane
	20	25	55
2 (VS)	toluene	methanol	cyclohexane
	35	25	40
3 (VS)	toluene	methanol	cyclohexane
	55	25	20
4 (MMBA)	fullerene	tetralin	toluene
	0.07	60	39.93
5 (HB, FC)	polystyrene	toluene	cyclohexane
	(MW 4730 g/mol)		
	2	39	59
6 (HB, FC)	polystyrene	toluene	
	(MW 4730 g/mol)		
	2	98	–

until 4th March 2019. All the experiments were handled by the Spanish User Support and Operations Center (E-USOC) in Madrid.

As described in more details in the literature [9,13, 27], in DCMIX campaign each cell array contains five ternary samples and one binary reference sample. The two-colour interferometer is equipped with two lasers of $\lambda_1 = 670\,\text{nm}$ (moving red, MR) and $\lambda_2 = 935\,\text{nm}$ (moving near-infrared, MN) wavelength, while the one-colour setup only contains the red source (fixed red, FR). The Soret cell is made of quartz glass and has a square cross section of $10 \times 10\,\text{mm}^2$ and a height of 5.0 mm along the direction of the temperature gradient. More details of the SODI hardware can be found in the literature [9,28,29].

The timeline of a typical run consists of two steps of equal duration: the isothermal step and the Soret step. During the initial isothermal step a uniform temperature is applied to a specific cell, in order to homogenize the sample under investigation by both temperature and concentration. Then, a temperature gradient is applied for the second step, with programmed acquisition of images, until the system reaches a steady state where the Soret counter-diffusion is balanced by the diffusive Fickian flux and an almost linear concentration gradient is obtained within the cell. The duration of the Soret step has been estimated on the basis of available literature data, by calculating the characteristic diffusion time τ_D from the smaller eigenvalue of the diffusion matrix. Then, the duration of the separation step was defined as about 10 times τ_D. In some cases, when no reference data was available, the timing was defined with some safety margins. At the end, the runs with different cells had very different duration, from several hours to a few days, according to the above definitions.

Table 2. List of the runs used for the preliminary analysis. Notation XrYZ for Run ID means: X is the cell number, YZ is the serial number of the experiment in the cell X.

Run #	Run ID	Cell #	T_{mean} (°C)	ΔT (°C)	Duration (h)
1	3r03	3	25	5	12
2	4r01	4	25	5	24
3	1r01	1	20	2	24
4	3r01	3	20	5	12
5	4r02	4	30	5	24
6	1r02	1	25	2	24
7	4r03	4	35	5	24
8	1r03	1	30	2	24
9	2r01	2	20	2	16
10	3r02	3	22.5	5	12
11	2r02	2	22.5	2	16
12	3r04	3	27.5	5	12
13	5r01	5	20	5	48
14	2r03	2	25	2	16
15	3r05	3	30	5	12
16	5r02	5	25	5	39.25
17	2r04	2	27.5	2	10.55
25	4r05	4	25	5	24

Experiments are automatically run in a previously established sequence with different average temperatures and/or temperature gradients as well as with different durations, depending on the specific sample. It is worth noting that experiments in the cells #5 and #6 were always running simultaneously, and with identical control parameters. A total of 58 runs have been conducted for DCMIX4, followed by several nice-to-have runs carried out at the completion of the program.

Every "data point" acquired during a run corresponds to two stacks of images, one for each wavelength, while an image stack includes five fringe images with a phase shift of $\pi/2$ between consecutive images, as accomplished by current-shifting of the laser sources. For each experiment thousands of image stacks are acquired and stored on dedicated flash disks that are exchanged by astronauts when full. Additionally, sample images are downloaded to earth by telemetry capabilities of the ISS. Typical downloaded sequences are in the order of 100 image stacks for each experimental run. In this paper we describe the control analysis performed on some of the sequences downloaded for runs 1–17 plus run 25, as carried out during the period from 14th December 2018 to 25th January 2019, while the experiment was still running. Most of the analysed runs belong to the time slot between the start of the mission and the first replacement of the flash disk storing the data. This data became available first; furthermore, the experiments at a mean temperature of 25 °C, which could be directly compared with available literature data and ongoing ground tests, fall mainly into this time slot. This

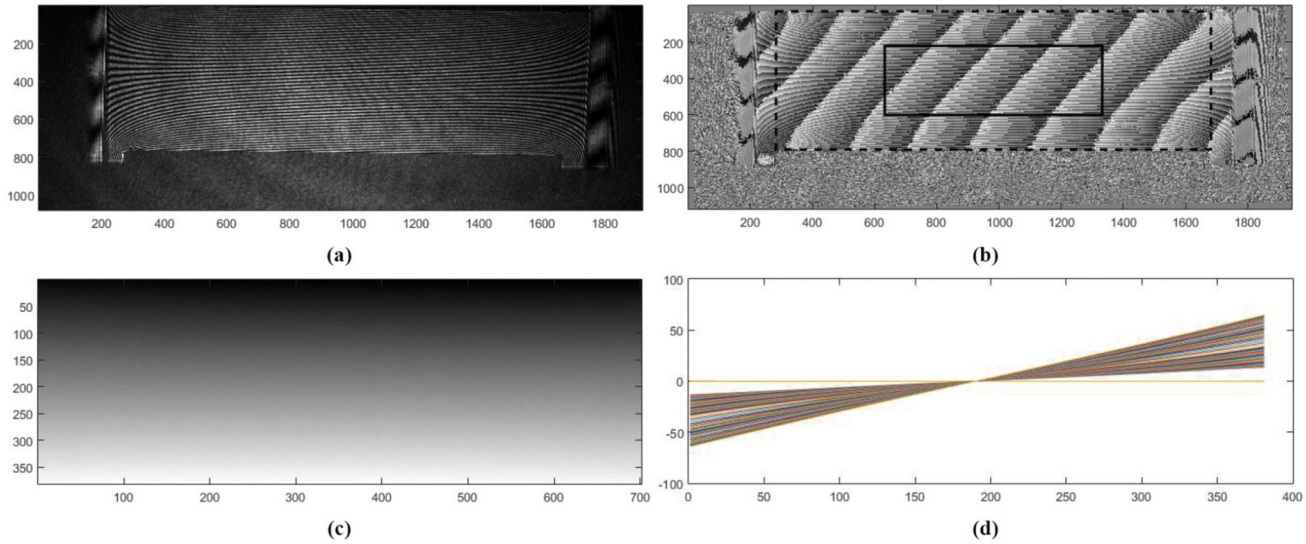

Fig. 2. Interferometry of a thermal field. From top to bottom, from left to right; (a) 1 image of a stack of the run #3 recorded with the MN laser, (b) rotated wrapped phase map, (c) unwrapped phase map, (d) phase profiles averaged over all the horizontal length of the ROI *vs.* height.

preliminary analysis on telemetry data was performed in order to check the quality of the running experiments and, if necessary, take actions to modify the foreseen sequence of experimental runs. In table 2 a summary of the analysed runs is provided.

3 Data analysis

3.1 Optical phase analysis of a temperature field

The DCMIX experiments are meant to measure transport properties such as mass diffusion and thermodiffusion coefficients of ternary mixtures by means of the optical digital interferometry technique. The full data analysis consists of two independent tasks: transferring the acquired images into the variation of refractive index and retrieving the diffusion and Soret coefficients from these data by fitting to analytical solutions. The refractive index changes both due to variations of the temperature and the concentrations and this induces a phase change of the interferograms recorded by the detector. The images analysis procedure is then based on the phase change analysis as further explained below.

To obtain the optical phase from the stack of interferograms the following equation is applied [30]:

$$\Phi(x,z,t) = \arctan\left[\frac{7(I_4 - I_2)}{4I_1 - I_2 - 6I_3 - I_4 + 4I_5}\right], \qquad (1)$$

where $\Phi(x,z,t)$ is the optical phase in the plane parallel to the applied temperature gradient and $I_i = I_i(x,z,t)$ are the intensities at pixel (x,z) of the image i of the stack recorded at the instant t.

In panel (a) of fig. 2 a sample image from the run #3 is reported. It can be seen that the image is slightly larger than the cell size, so that the laterally confining glass windows are clearly visible. The five fringe images of each stack are used to compute the phase map through eq. (1). The phase map is typically slightly tilted with respect to horizontal due to misalignment between the cell and the optics. Therefore, difference phase map is rotated by an angle custom detected for every cell, the misalignment being different, in general, for each cell. Then, a region of interest (ROI) is selected within each phase map. Here the ROI has been chosen to be 50% of the size of the cell both in the vertical and in the horizontal direction, thus covering 25% of the full area. In panel (b) of fig. 2 a rotated phase map can be observed with a superimposed dashed rectangle showing the detected area of the cell and a continuous line smaller rectangle showing the ROI utilized in the following. The phase maps obtained through the algorithm of eq. (1) are wrapped phases, *i.e.* they are mathematically bounded within $-\pi$ and π. The real phase map then needs to be unwrapped in order to get the continuous phase map. This is done by means of routine 2D-unwrapping algorithms and the result is shown in panel (c) of fig. 2. The detailed description of the image processing can be found elsewhere [28,31]. Finally, the phase map is averaged in the x-direction (horizontal in the image) and difference phase profiles $\Phi(z,t)$ are obtained for each image stack and shown in panel (d) of fig. 2. The profile is almost flat for times earlier than the application of the thermal gradient.

3.2 Control of thermodiffusion process by interferometry

The phase map abruptly changes when a temperature gradient is applied, because the limited number of downloaded control images does not allow to accurately track the dynamics of the temperature field development in the liquid.

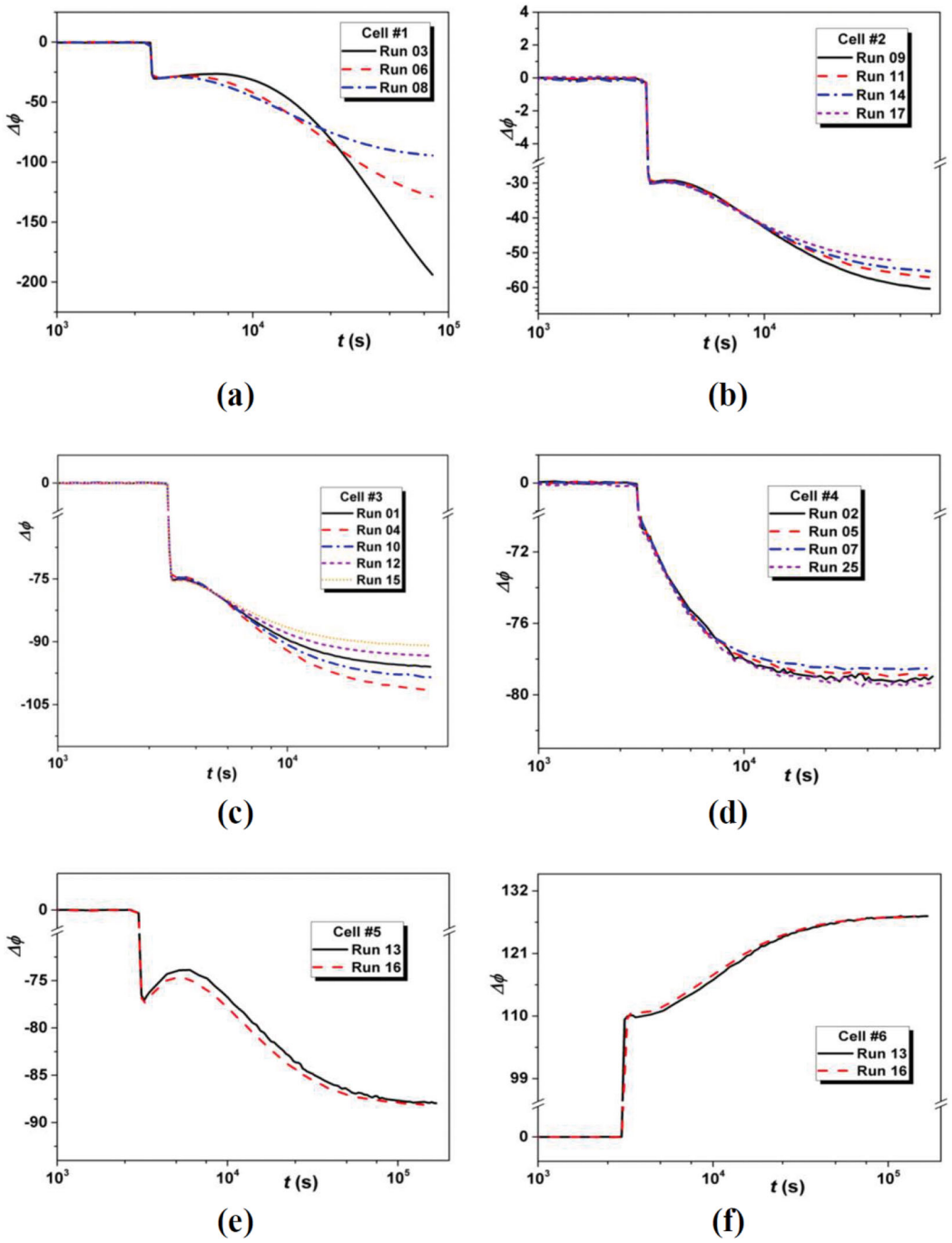

Fig. 3. Log-lin plot of the phase difference between top and bottom of the ROI *vs.* time recorded with the MN laser for cells #1–5 and FR laser for cell #6.

The Soret effect induces components separation and the concentration fronts slowly move within the sample from the horizontal walls toward the cell center, as mirrored by the change of the difference phase map. The phase difference $\Delta\Phi(t)$ is calculated by taking the difference between top and bottom values of the phase.

The same procedure is applied for all the runs. As this is a first estimation, only images recorded with the moving near-infrared laser were used for cells 1 to 5 (ternary mixtures). For the companion cell (binary mixture), only images recorded with the fixed red (FR) laser are available. We report below the result for the following runs:

In fig. 3(a) for the cell #1 (runs 3, 6 and 8).
In fig. 3(b) for the cell #2 (runs 9, 11, 14, 17).
In fig. 3(c) for the cell #3 (runs 1, 4, 10, 12, 15).
In fig. 3(d) for the cell #4 (runs 2, 5, 7, 25).
In fig. 3(e) for the cell #5 (runs 13 and 16).
In fig. 3(f) for the cell #6 (runs 13 and 16).

3.3 Quantitative results on separation and diffusion

Apart from the qualitative analysis of raw optical phase of all the cells, we have also performed an exploratory quantitative analysis of selected cells and runs. In this analysis we have focused exclusively on the Soret separation step of a run and evaluated only the optical signal related to concentration variations in the studied mixture. The related procedure was more complex and consisted in several additional steps:

- obtaining a set of vertical profiles of the unwrapped optical phase at centreline of the cell's ROI, $\Phi(x = L/2, z, t)$;
- selection of a proper reference phase profile $\Phi(z, t_0)$ and finding its correct timestamp t_0 with respect to the reference time $t = 0$ when the temperature gradient is switched on. This time t_0 is a nearest time instant, at which the thermal field inside the cell can be considered as *completely established*;
- subtraction of the reference phase profile from all subsequent phase profiles of the Soret step, with the purpose of obtaining the phase variation related to concentration, $\Phi'(z, t_i \geq t_0) = \Phi(z, t_i) - \Phi(z, t_0)$;
- conversion of such calculated optical phase into refractive index, $n'(z, t) = (\lambda/2\pi L)\,\Phi'(z, t)$;
- fitting of all experimental profiles $n'(z, t)$ obtained during Soret step to one of possible analytical solutions describing separation in this geometry. Accuracy of the fit is essentially improved if the initial time t_0 is explicitly accounted for in the procedure (more details can be found elsewhere [28]).

An approach that has been adopted for the last step of fitting was that of considering the ternary mixture as a quasi-binary one, which reduces the number of fitting parameters to only two: steady-state separation as measured by refractive index Δn^{st}, and effective quasi-binary diffusion coefficient D_{qb}. Of course, the major concern for applying such approach to true ternary mixtures is that two kinetics do contribute to the separation curve, as determined by the two eigenvalues $\hat{D}_1$ and $\hat{D}_2$ of the diffusion matrix. Indeed, the approach has to be used with care; but according to our experience, the two kinetics become distinguishable in very rare and particular cases: when magnitudes of eigenvalues are very different, and when amplitudes of the related kinetics are comparable and/or these amplitudes have opposite signs, as happens in cell #5 (see fig. 3(e)). This condition is not fulfilled in many practical cases, and as a result, the quasi-binary fit does usually provide very good approximation to the separation in a ternary mixture. A value of the quasi-binary diffusion coefficient D_{qb} obtained from the fitting, as a rule, it is closer to the smaller eigenvalue.

This approach has been applied for analysis of diffusion in the three cells containing toluene-methanol-cyclohexane mixtures, and results have been compared with literature data available for 25 °C. Figure 4 shows the evolution of the smallest eigenvalue approaching to the demixing zone at $T_{mean} = 25\,^{\circ}\mathrm{C}$. Red filled squares

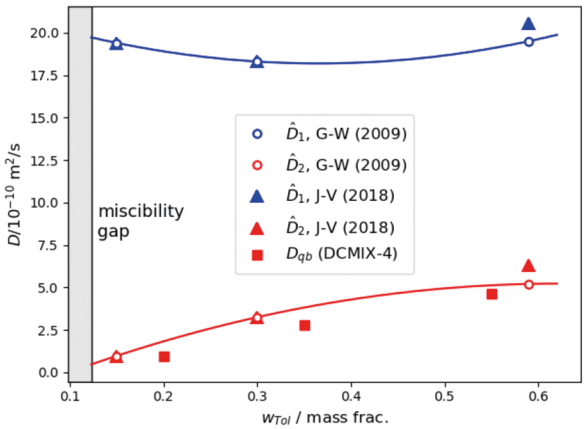

Fig. 4. Diffusion in three cells filled with the toluene-methanol-cyclohexane mixture at mean temperature 25 °C, compared with eigenvalues of the diffusion matrix from the literature [18, 19,32]. The microgravity results in the cells #1, #2 and #3, for runs 6, 14 and 1, respectively (filled squares) are obtained by processing images acquired with MN laser.

correspond to results obtained on the ISS while the open circles correspond to ground measurements by Grossman & Winkelmann, 2009. The ground and microgravity results are in excellent agreement for the smallest eigenvalue. We also added the results obtained by molecular dynamic simulations [32]. For the smallest eigenvalue they highlight the good quality of microgravity results and for the largest eigenvalue they are in line with ground measurements. Two conclusions can be drawn out of these preliminary results: first, the smallest eigenvalue decreases towards the demixing zone; second, the two eigenvalues are very different: for the mixture poor in toluene they differ by more than ten times. It is worth noting that the results clearly demonstrate that quasi-binary approach works well despite the large difference in eigenvalues and provide the diffusion coefficient D_{qb} very close to the smallest eigenvalue.

The same approach was applied for cell #4 which, presumably, has close eigenvalues. Figure 5 (top and middle panels) show an example of the different way of the fitting aimed to get the value of Δn^{st} and D_{qb}. The example is given for the cell #4, run 25 at mean temperature of 25 °C. In the first case (top panel) these quantities are determined from the full profiles $n(z, t)$ across the cell and in the second case (middle panel) the gradient of the refractive index in the central part of the cell (over a layer of 2 mm) is used for fitting. The analytical solutions used in fitting for both approaches can be found in ref. [12]. Both approaches provide rather similar values for both quantities. For example, the values of diffusion coefficients are $D_{qb,full} = 8.5 \cdot 10^{-10}\,\mathrm{m}^2/\mathrm{s}$ and $D_{qb,grad} = 8.8 \cdot 10^{-10}\,\mathrm{m}^2/\mathrm{s}$.

In the case of the polymeric ternary mixture of cell #5 the two kinetics of the mass separation are expected to be quite different due to the large difference between the molecular weights of the components. As can be seen in fig. 3(e), for this cell, after an abrupt negative variation of the phase difference due to the application of the thermal

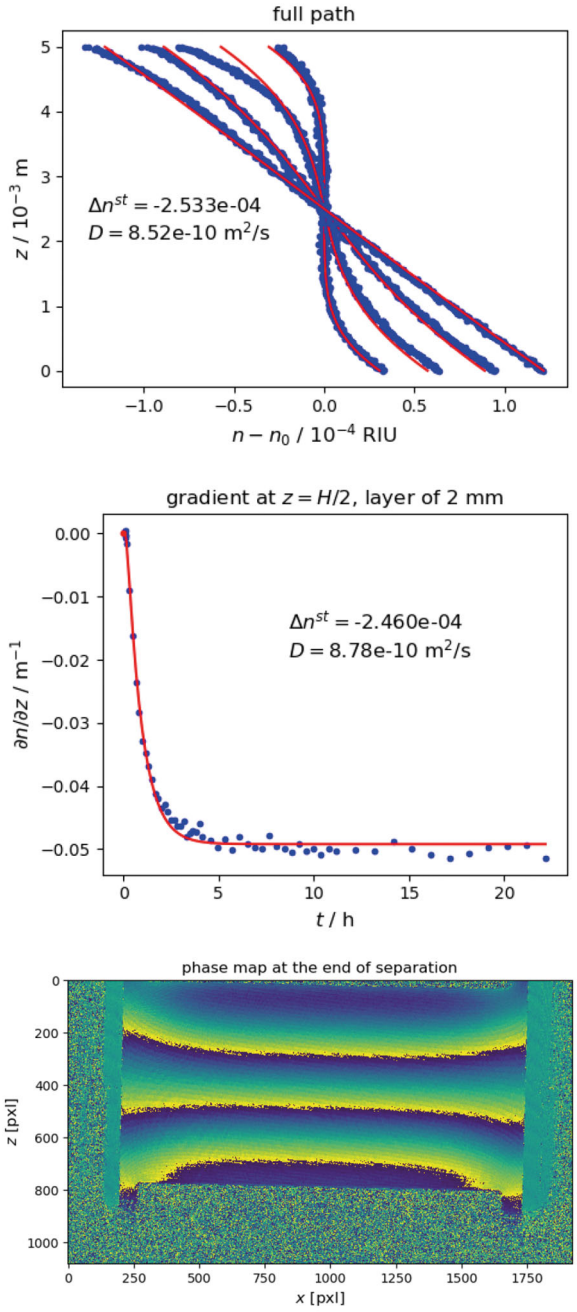

Fig. 5. The separation and diffusion results in the cell #4 filled with fullerene-tetralin-toluene (run 25) obtained from images of MR laser. Top: vertical profiles of the refractive index $n(z)$ in the cell center as a function of time. Middle: temporal variation of $\partial n/\partial z$; in both cases the blue points show the experimental point and red curves correspond to the fitting. Bottom: phase map at the end of observation.

gradient, a positive variation occurs followed by a slower negative variation. These two variations of opposite directions are compatible with Soret coefficients of opposite sign, as expected for the polystyrene-toluene-cyclohexane mixture, since toluene-cyclohexane has a negative Soret coefficient [16] while polystyrene-toluene mixtures typically show positive Soret coefficient [33]. In this case, even with only one wavelength, thanks to the well distinguishable dynamics, one can determine the two eigenvalues of the diffusion matrix of the ternary mixture. However, a more detailed and complete analysis is needed and we will provide it in a future publication.

For cell #6 (see fig. 3(f)), after a fast positive variation of the phase difference relative to the imposition of the thermal gradient, a unique and positive variation of the phase difference is observed. This is expected since the investigated sample is the reference binary mixture for the DCMIX4 experiment. With a binary analysis we obtain a diffusion coefficient of $D = 2.2 \cdot 10^{-10}\,\mathrm{m}^2/\mathrm{s}$, quite compatible with the value measured for the same binary mixture, but by dynamic analysis of the light scattered by the non-equilibrium fluctuations of the density [34].

4 Parameter modification

The first results obtained from the presented preliminary analysis of the images downlinked in near real-time in the course of the experiment revealed that most of the experimental runs are working nominally, which means that DCMIX4 is successfully progressing. At the time of submission of the present paper, similar analysis was performed on all the 58 runs and a global success of the experimental campaign is confirmed.

We have to particularly underline, that this success resulted essentially from a close collaboration between the scientific team, space research office of ESA, engineers of the company-manufacturer of the instrument (QinetiQ Space) and the user-support team. This collaboration, with rapid information exchange, fast notification of problems and instant feedbacks, allowed to minimize the time needed for the initiation and maintenance of the experiment, in favour of the science runs. Periodic screening on the fly has shown that all samples were bubble-free all over the full experiment, as during the scheduled runs bubbles did not appear in any cell.

Following the simplified analysis reported above, the science team has also recognized the slowing-down of the diffusion process in cell #1 (closest to phase separation) with the decrease of the temperature from 30 °C to 20 °C, an effect which was difficult to estimate beforehand. Its accurate analysis is outside the scope of the present paper and will be presented at a later stage.

This preliminary analysis allowed pointing out that the total time of the runs of cell #1 (see fig. 3(a)) should be extended, in particular for low mean temperatures, in order to reach a stationary state and fully evaluate the Soret coefficients. It was proposed to increase the duration of the cell #1 runs at $T_{mean} < 25\,^{\circ}\mathrm{C}$ and to repeat the runs already performed at a lower temperature. It was also suggested measuring thermodiffusion at a slightly lower mean temperature, further approaching the demixing zone, and to do it at the end of all experiments, in order to avoid risks related to demixing. A slightly longer duration was also requested for cell #2 in experiments with a low temperature. Based on the experience from past missions,

E-USOC had developed an operations concept and tools that ensured a flexible planning and commanding of the instrument. This, together with the fluid communication between E-USOC, the scientific team and ESA, allowed to successfully accomplish these changes in the parameters and additional runs during the execution of the experiment, without compromising the mission success or its assigned on board timeframe.

During nice-to-have runs in the cell #1, demixing was observed when the mean temperature was lowered to 17.5 °C at $\Delta T = 2$ °C. This means that the bottom wall had a temperature of 16.5 °C and the mixture was at the border of the demixing zone.

5 Conclusions

We have presented a preliminary evaluation of the results of the DCMIX4 experiment performed on board the ISS as obtained by analyzing telemetry images downloaded during the first weeks of the on-orbit campaign. The telemetry images allowed us to qualitatively assess the performance of the experiments by evaluating the amplitude of the signal and the ability of the procedure to extract the relevant information. Such preliminary analysis also allowed us to check that no gas bubble was present in any sample cell. Moreover, from studying these images we could judge whether the time prescribed for the experiments was sufficient for the duration of the phenomena under study. This inspection allowed modification of the adjustable parameters in order to fully take advantage of the unique experimental conditions of the ISS. Results related to all cells have been assessed as of sufficiently quality for future complete analysis when all images will be available by physically downloading data discs from the ISS to Earth.

FC, HB and LGF acknowledge financial support from the Centre National d'Etudes Spatiales (CNES) and from the funding partners of the Industrial Chair CO2ES: E2S-UPPA, TOTAL, CNES and BRGM. AM, YG and VS acknowledge support by the PRODEX program of the Belgian Federal Science Policy Office. MMBA and AE acknowledge support of FETRAFLU (2018-CIEN-000101-01) from Gipuzkoa Program for Science, ATNEMFLU (ESP2017-83544-C3-1-P) of the MINECO and the Research Group Program (IT1009-16) from the Basque Government.

Author contribution statement

AM, HB, MMBA, MB, FC, LGF and VS participated in the experiment planning, selection of liquids and definition of the experimental parameters. AM, HB, MMBA, FC, AE, YG, LGF and VS were responsible for the flight samples preparation. JR, JME and JJF performed the data collection of the experiments by implementing and executing the experimental campaign on board the ISS. MB ensured the coordination of the experiment-related activity. AM, HB, MMBA, FC, AE, YG, LGF and VS analyzed the data, performed the image processing and discussed the results. AM, HB, MMBA, FC, LGF, JR and VS wrote the manuscript. All authors discussed the content of the paper.

References

1. J.K. Platten, J. Appl. Mech. **73**, 5 (2005).
2. J. Platten, M. Bou-Ali, P. Costeséque, J. Dutrieux, W. Köhler, C. Leppla, S. Wiegand, G. Wittko, Philos. Mag. **83**, 1965 (2003).
3. W. Köhler, K. Morozov, J. Non-Equilib. Thermodyn. **41**, 151 (2016).
4. A. Leahy-Dios, M.M. Bou-Ali, J.K. Platten, A. Firoozabadi, J. Chem. Phys. **122**, 234502 (2005).
5. M. Bou-Ali, J. Platten, J. Non-Equilib. Thermodyn. **30**, 385 (2005).
6. P. Blanco, M.M. Bou-Ali, J.K. Platten, D. Alonso de Mezquia, J.A. Madariaga, J. Chem. Phys. **132**, 114506 (2010).
7. A. Königer, H. Wunderlich, W. Köhler, J. Chem. Phys. **132**, 174506 (2010).
8. M. Braibanti *et al.*, Eur. Phys. J. E **42**, 86 (2019).
9. A. Ahadi, S. Van Vaerenbergh, M.Z. Saghir, J. Chem. Phys. **138**, 204201 (2013).
10. Q. Galand, S. Van Vaerenbergh, W. Köhler, O. Khlybov, T. Lyubimova, A. Mialdun, I. Ryzhkov, V. Shevtsova, T. Triller, submitted to J. Chem. Phys. (2019).
11. A. Mialdun, V. Shevtsova, J. Chem. Phys. **143**, 224902 (2015).
12. A. Mialdun, I. Ryzhkov, O. Khlybov, T. Lyubimova, V. Shevtsova, J. Chem. Phys. **148**, 044506 (2018).
13. T. Triller, H. Bataller, M.M. Bou-Ali, M. Braibanti, F. Croccolo, J.M. Ezquerro, Q. Galand, J. Gavaldá, E. Lapeira, A. Laverón-Simavilla, T. Lyubimova, A. Mialdun, J.M. Ortiz de Zárate, J. Rodríguez, X. Ruiz, I.I. Ryzhkov, V. Shevtsova, S. Van Vaerenbergh, W. Köhler, Micrograv. Sci. Technol. **30**, 295 (2018).
14. M.M. Bou-Ali, A. Ahadi, D. Alonso de Mezquia, Q. Galand, M. Gebhardt, O. Khlybov, W. Köhler, M. Larrañaga, J.C. Legros, T. Lyubimova, A. Mialdun, I. Ryzhkov, M.Z. Saghir, V. Shevtsova, S. Van Vaerenbergh, Eur. Phys. J. E **38**, 30 (2015).
15. M. Gebhardt, W. Köhler, J. Chem. Phys. **142**, 084506 (2015).
16. E. Lapeira, M. Gebhardt, T. Triller, A. Mialdun, W. Köhler, V. Shevtsova, M.M. Bou-Ali, J. Chem. Phys. **146**, 094507 (2017).
17. T. Janzen, S. Zhang, A. Mialdun, G. Guevara-Carrion, J. Vrabec, M. He, V. Shevtsova, Phys. Chem. Chem. Phys. **19**, 31856 (2017).
18. T. Grossmann, J. Winkelmann, J. Chem. Eng. Data **54**, 405 (2009).
19. T. Grossmann, J. Winkelmann, J. Chem. Eng. Data **54**, 485 (2009).
20. C.I.A.V. Santos, V. Shevtsova, A. Ribeiro, Eur. Phys. J. E **40**, 40 (2017).

21. E. Castro, A. Hernandez Garcia, G. Zavala, L. Echegoyen, J. Mater. Chem. B **5**, 6523 (2017).
22. J. Lee, S. Cho, Y. Hwang, H.J. Cho, C. Lee, Y. Choi, B.C. Ku, H. Lee, B. Lee, D. Kim, S. Kim, Tribol. Int. **42**, 440 (2009).
23. D. Guldi, B. Illescas, C. Atienza, M. Wielopolski, N. Martín, Chem. Soc. Rev. **38**, 1587 (2009).
24. H. Bataller, T. Triller, B. Pur, W. Köhler, J.M. Ortiz de Zárate, F. Croccolo, Eur. Phys. J. E **40**, 35 (2017).
25. A. Vailati, R. Cerbino, S. Mazzoni, C.J. Takacs, D.S. Cannell, M. Giglio, Nat. Commun. **2**, 290 (2011).
26. F. Croccolo, C. Giraudet, H. Bataller, R. Cerbino, A. Vailati, Micrograv. Sci. Technol. **28**, 467 (2016).
27. V. Shevtsova, C. Santos, V. Sechenyh, J.C. Legros, A. Mialdun, Micrograv. Sci. Technol. **25**, 275 (2014).
28. A. Mialdun, J.C. Legros, V. Yasnou, V. Sechenyh, V. Shevtsova, Eur. Phys. J. E **38**, 27 (2015).
29. T. Triller, *Diffusive properties of the system water/ethanol/triethylene glycol in microgravity and ground conditions*, Doctoral Thesis, University of Bayreuth, Faculty of Mathematics, Physics and Computer Sciences, Bayreuth, Germany (2018) URL: `https://epub.uni-bayreuth.de/3861/`.
30. T. Kreis, *Handbook of Holographic Interferometry: Optical and Digital Methods* (Wiley, VCH Verlag GmbH & Co. KGaA, Weinheim, 2005)
31. A. Mialdun, V. Shevtsova, J. Chem. Phys. **134**, 044524 (2011).
32. T. Janzen, J. Vrabec, Ind. Eng. Chem. Res. **57**, 16508 (2018).
33. J. Rauch, W. Köhler, J. Chem. Phys. **119**, 11977 (2003).
34. F. Croccolo, L. García-Fernández, H. Bataller, A. Vailati, J.M. Ortiz de Zárate, Phys. Rev. E **99**, 012602 (2019).